Microsecond switchable thermal antenna

Philippe Ben-Abdallah, Henri Benisty, Mondher Besbes

Microsecond switchable thermal antenna

Philippe Ben-Abdallah,[a] Henri Benisty, and Mondher Besbes
Laboratoire Charles Fabry, UMR 8501, Institut d'Optique, CNRS, Université Paris-Sud 11, 2, Avenue Augustin Fresnel, 91127 Palaiseau Cedex, France

(Received 22 March 2014; accepted 7 July 2014; published online 17 July 2014)

We propose a thermal antenna that can be actively switched on and off at the microsecond scale by means of a phase transition of a metal-insulator material, the vanadium dioxide (VO_2). This thermal source is made of a periodically patterned tunable VO_2 nanolayer, which support a surface phonon-polariton in the infrared range in their crystalline phase. Using electrodes properly registered with respect to the pattern, the VO_2 phase transition can be locally triggered by ohmic heating so that the surface phonon-polariton can be diffracted by the induced grating, producing a highly directional thermal emission. Conversely, when heating less, the VO_2 layers cool down below the transition temperature, the surface phonon-polariton cannot be diffracted anymore so that thermal emission is inhibited. This switchable antenna could find broad applications in the domain of active thermal coatings or in those of infrared spectroscopy and sensing. [http://dx.doi.org/10.1063/1.4890517]

I. INTRODUCTION

A thermal antenna is a spatially coherent source that radiates in the infrared or the mid-infrared frequency range. In 1988, after a pioneering work of Hesketh *et al.*[1] on the radiant modes of periodic micromachined silicon surfaces, the first thermal antenna has been designed using deep gratings.[2] Since then, numerous directional thermal sources and partially coherent sources have been proposed by texturing materials at subwavelength scale.[3–13] However, to date, no antenna that operates in the infrared range, can be actively controlled without moving parts and the emission patterns of existing sources remain time-invariant. There are many applications that would profit by quickly variable, temporally agile thermal radiation sources. Sources for spectroscopy are a simple example, modulation being an obvious advantage in most measurement techniques. There are many other technological opportunities that would benefit from an active thermal coating with dynamics in the 1 s…μs range.

No solution had emerged in this context that would get beyond the limits of thermal or mechanical inertia characteristic times (typically > 1 s), but an important step toward temporal control has been recently achieved in a closely related study area. Specifically, a strategy was proposed to temporally modulate the near-field heat flux exchanged between two hot bodies[14,15] by using insulator-metal transition (MIT) coatings deposited on the exchange surfaces of these facing bodies. By passing an MIT material from its crystalline phase to its amorphous state, its optical properties can be very significantly modified. This bifurcation in the optical behavior of MIT materials has been recently exploited to propose efficient radiative thermal rectifiers[16] and near-field thermal transistors.[17] Hence, the topic of the present work is connected to novel physical configurations as well as devices and notably MEMs (micro-electro-mechanical systems), where time scales have not been explicitly specified. A typical MEMs membrane has a relatively low inertia, with frequency up to 20 Hz thermal modulation bandwidth reported with adequate cooling channels. It should also be stressed here that the rise time of the phase transition can be very quick if it is electrically induced, for instance, falling well below the microsecond rate. Thin layers on top of a substrate will be seen in the following to have cycle times (rise and fall times) of a couple of microseconds typically.

In this paper, we introduce a switchable thermal antenna by exploiting these phase transitions. It is basically composed of an MIT material that supports a surface wave in the frequency range of emission (Planck's window) of the antenna. By an appropriate addressing of regions where transition is triggered, a grating can be generated on the crystalline phase of MIT material so that the surface wave can be diffracted, on-demand, into the far field, making the emission pattern highly directional. Also, we show that the direction of emission can be controlled and the thermal emission itself can be switched off or switched on by making appropriate local phase transitions.

In a first part, we describe the thermal emission properties of a simple untextured MIT material in its two phases, cristalline and amorphous, choosing the most common case of vanadium dioxide (VO_2). Then, we show that this material supports, in its monoclinic (anisotropic) phase, a surface phonon-polariton (SPP) that inhibits the thermal emission in the far-field. Conversely, when a grating is imprinted onto the MIT by a local phase transition, the thermal emission becomes large and highly directional. Finally, we show that the emission pattern of this source can be tuned above on the time scale of a few microseconds by dynamically changing the surface grating geometry, at a timescale comparable to the short time of thermal relaxation of VO_2 nanolayers.

[a]Electronic mail: pba@institutoptique.fr

II. THERMAL EMISSION OF BULK VO_2

Let us start by considering a semi-infinite sample of VO_2, an MIT material, whose critical temperature is $T_c = 340\,\mathrm{K}$, the other half-space being just vacuum. Below T_c, this material is in its crystalline (monoclinic) phase, forming thus a uniaxial medium. The dielectric permittivities VO_2 coming from reflection measurements[18] and by ellipsometry[19] in both phases are plotted in Fig. 1. In the cristalline phase, we denote by $\epsilon_\perp$ its value along the optical axis, and by $\epsilon_\parallel$ its value in the plane orthogonal to it. Experimental data show that the optical axis is, in most occurrences, orthogonal to the surface so that $\epsilon_\parallel$ corresponds to the permittivity in the plane parallel to the surface. In such crystals, the reflection coefficients for s (TE) and p (TM) polarizations are given[20] by the following expressions:

$$r_l^{s,s} = \frac{k_{z0} - k_{z;s}}{k_{z0} + k_{z;s}}, \tag{1}$$

$$r_l^{p,p} = \frac{\epsilon_\parallel k_{z0} - k_{z;p}}{\epsilon_\parallel k_{z0} + k_{z;p}}, \tag{2}$$

where $k_{z;s,p}$ are solutions of the Fresnel equation

$$\left(\epsilon_\parallel \frac{\omega^2}{c^2} - \kappa^2 - k_{z;s}^2\right)\left(\epsilon_\parallel \epsilon_\perp \frac{\omega^2}{c^2} - \epsilon_\parallel \kappa^2 - \epsilon_\perp k_{z;p}^2\right) = 0. \tag{3}$$

In these relations, $k_{z0} = \sqrt{\omega^2/c^2 - \kappa^2}$ denotes the normal component of wavevector in the surrounding medium (vacuum), while κ stands for the parallel component of wavevector.

It immediately follows by inspection of these reflection coefficients and of their poles that only p-polarized surface waves can exist at the interface of these media (see Fig. 2). Their dispersion relation reads

$$\kappa = \frac{2\pi}{\lambda}\sqrt{\frac{(\epsilon_\parallel - 1)\epsilon_\perp}{\epsilon_\parallel \epsilon_\perp - 1}}. \tag{4}$$

Since VO_2 is a polar material, these surface waves are SPP. The dispersion relation of a resonant SPP mode is plotted in Fig. 2 in the mid-infrared range. This SPP is spectrally localized at the wavelength where a horizontal asymptote around $\lambda = 6\,\mu\mathrm{m}$ appears, which corresponds to the region where the density of states becomes very high. The precise location of the SPP asymptote can be analytically determined from expression (4) by solving $\epsilon_\parallel \epsilon_\perp = 1$. The emission patterns plotted in Fig. 3 shows the inhibiting role of the SPP on thermal emission for the purely crystalline phase. Note that Fig. 3(a) peaks at only 3.6%. Since the incident (propagative) light cannot couple with the sample at the SPP wavelength, it is reflected so that, according to Kirchoff's law, the emission is weak. In its amorphous phase, no SPP exists.

However, the thermal emission still remains small at normal incidence because $|\epsilon_m|$ is very large (see Fig. 1) so that the reflection coefficient is close to unity. On the other hand, at oblique incidence, near $\theta = 85^\circ$, a large thermal emission is recovered. This specific angle corresponds to the Brewster angle of amorphous VO_2, where the reflection vanishes. In both phases, the thermal emission of VO_2 is, roughly speaking, Lambertian due to the absence of spatial correlation in the field radiated by the material.

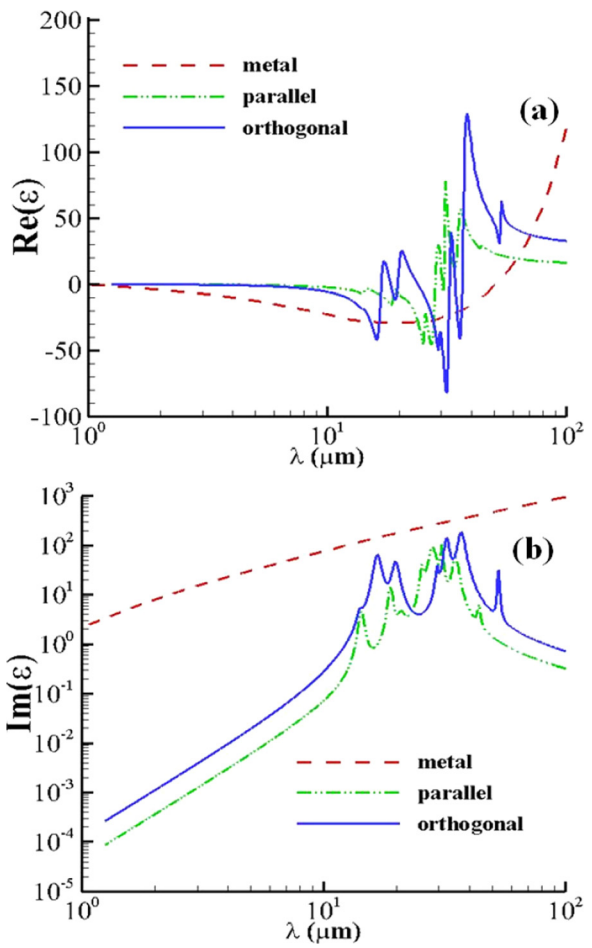

FIG. 1. (a) Real part of the permittivity ϵ_m of VO_2 in the metallic phase and of the permittivity $\epsilon_\parallel$ in the crystalline state along the plane and $\epsilon_\parallel$ and $\epsilon_\perp$ along the optical axis. (b) Imaginary part of the same quantities.

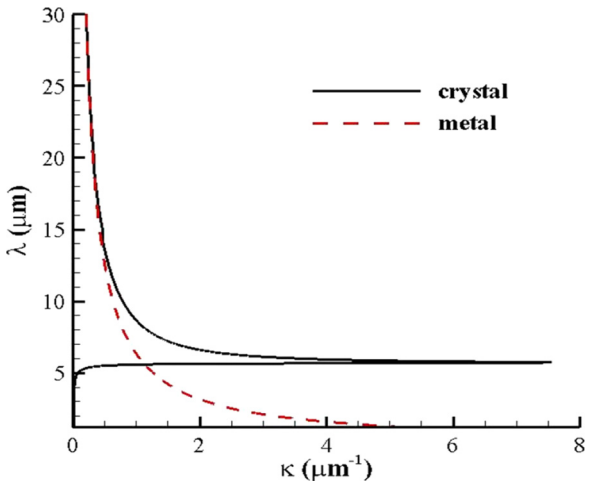

FIG. 2. Dispersion relation of surface modes of crystalline VO_2. In its amorphous (metallic) phase, VO_2 does not support any surface wave.

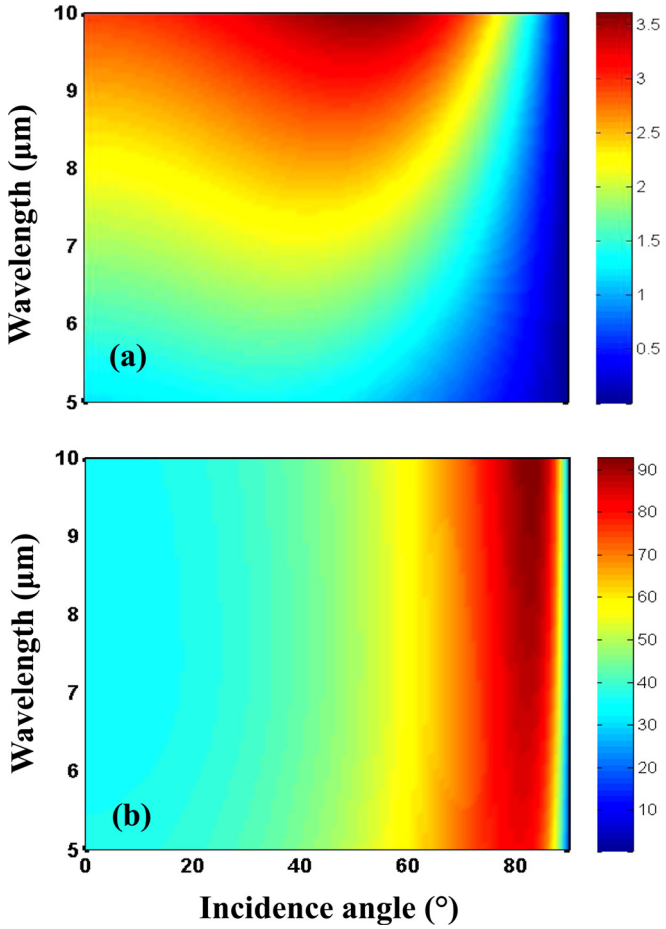

FIG. 3. Emissivity as a percent of a bulk VO_2 sample in (a) its crystalline and (b) its amorphous phases in TM polarization.

III. THERMAL EMISSION OF VO_2 GRATINGS

We now assume that some regions of VO_2 can be switched by Joule heating so as to transit from the crystalline state to the amorphous one. This can be done, for instance, by using a network of electrodes periodically distributed as illustrated in Fig. 4. Then, as we are going to see, depending on the shape of emitter, the far-field emission of the source can be switched between two radically different patterns. The grating depth is chosen identical to the attenuation length $\ell_{SPP} = [2\mathrm{Im}(k_{z;p})]^{-1}$ of SPP in the crystalline phase of VO_2, as this suffices to control the "local" SPP presence. As shown in Fig. 5, this corresponds to a thickness a little bit smaller than $\ell = 200\,\mathrm{nm}$ (far from the light line $\kappa = k_0$ all modes are confined at smaller distances than ℓ from the surface).

From a practical point of view, to prevent the phase transition in unwanted regions, a thin thermally insulating layer of silica[21] (typically, 20 nm thick of thermal conductivity $\kappa_{SiO_2} = 1.4\,\mathrm{W\,m^{-1}\,K^{-1}}$) is introduced between the substrate and the top region where the grating is induced by phase transition. Compared with the thermal conductivity of VO_2 ($\kappa_{VO_2} = 4\,\mathrm{W\,m^{-1}\,K^{-1}}$ Ref. 22) this conductivity is three times smaller and it ensures a sufficiently large thermal gradient to guarantee the temporal stability of both phases during the modulation process. It is important to outline here that the value of the thermal conductivity used in our simulations for the VO_2 layers is rather small compared with many reported measurements.[23] The variation of this property could either slow down or accelerate the dynamic of thermal relaxation process. However, our simulations have shown that the dynamic is not qualitatively affected by such variations. Note that the presence of an interface thermal resistance (not taken into account in our numerical simulations) between the silica layer and the VO_2 is a favourable effect, which maintains the grating interface invariant during a longer time intervalle. This layer makes the system slightly more complex, but even so the thermal emissivity ϵ of these sources in both configurations can be easily calculated from the rigorous coupled waves analysis (RCWA) method.[24] The results plotted in Fig. 6 in the (λ, θ) plane clearly show two radically different patterns.

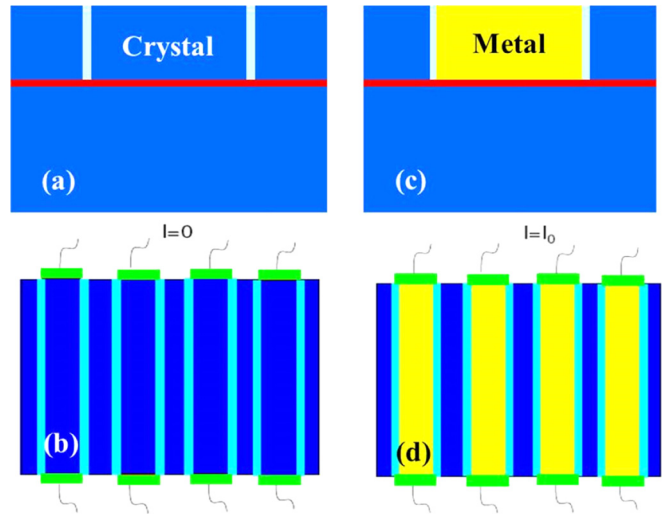

FIG. 4. Sketch of a thermal antenna based on phase transition materials. (a) and (b) the MIT material (side view) is in its crystalline phase and the source is non-radiating. (c) and (d) Top view of the antenna. The phase change is driven by an electrode network (in green) to generate a half-metallic surface grating. A 20 nm thick thermally and electrically insulating layer of silica (in red) separates the grating from the substrate, while grooves (in light blue) of 200 nm depth and 20 nm width filled by air separate all addressable VO_2 cells.

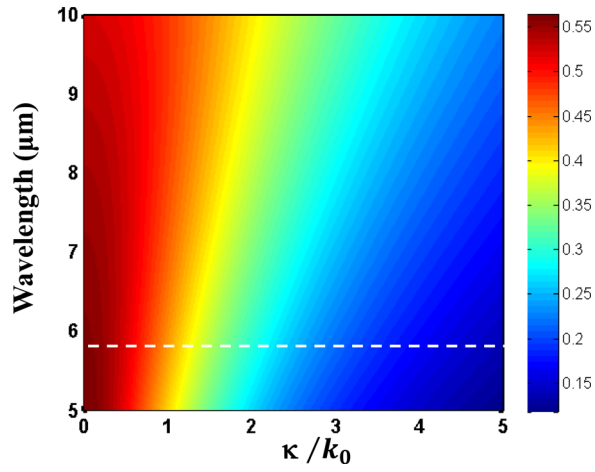

FIG. 5. Attenuation length (in micrometer) of modes in the crystalline phase of VO_2 around the SPP wavelength (horizontal dashed line).

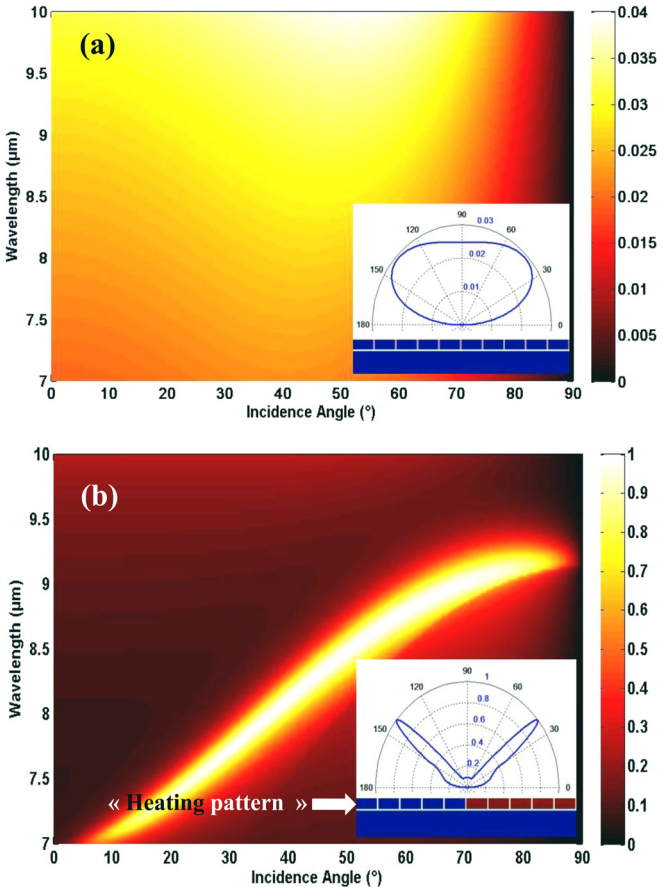

FIG. 6. TM-polarized emissivity of the VO_2-source in (a) its purely crystalline (dark blue) non-emitting phase and (b) in its hybrid (crystalline-amorphous) phase where the amorphous phase forms a surface grating of period $P_1 = 4.5\,\mu$m (10 unit cells of 450 nm length each). The inset shows the structure of one period of the source and its emission pattern at 8.5 μm.

When the source is in its crystalline state in all regions of space, the total thermal emission is very weak. As discussed in the previous section, this is consistent with the fact that the medium supports a surface wave so that the reflection coefficient is very large and therefore the absorption is weak. On the other hand, if we address some spatial regions so that a grating of VO_2 emerges whereby some cells are crystalline and other amorphous, then the emission pattern of the source becomes strongly directional, and the magnitude of emission peaks is close to unity. In Fig. 6, there are 5 out of 10 stripes that are heated (bottom of the inset). The exact amount of heat that shall cross boundaries between the two types of cells depends on how critical it is to attain well separated phases, thus, addressing the complex issue of hysteresis in relation with deposition technology. We discuss below typical geometric configurations which depend on the temperature gradient inside the structure.

We additionally show in Fig. 7 that we can also modulate the direction of emission of the antenna by addressing different VO_2 cells so as to adequately form the geometric features of the surface grating. In Fig. 7, there are now 6 heated stripes out of 12 (bottom of inset). According to grating theory, the emission direction is given by the Bragg relation[3]

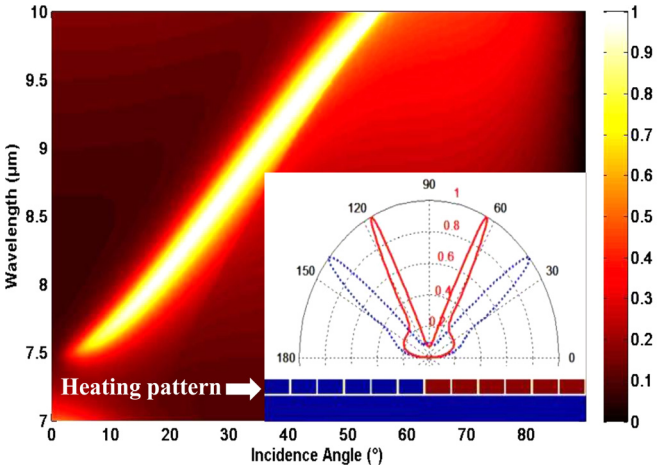

FIG. 7. Emissivity TM of the VO_2-source in its antenna mode with a surface grating of period $P_2 = 5.4\,\mu$m (12 unit cells of 450 nm length each). The inset shows the structural configuration of the source and its emission pattern at 8.5 μm as a solid red line. The blue dashed line, on the other hand, recalls the emission diagram at the same wavelength when the grating period is P_1 as in Fig. 6.

$$K_j = \frac{2\pi}{\lambda}\sin\theta + 2j\frac{\pi}{P}, \tag{5}$$

where K_j is the parallel component of wavevector diffracted in the *jth* order and P is the period of grating. Hence, the rather straightforward role of the period, obtained here as a multiple of the strip period. This is similar to what is done for more classical spontaneous sources such as luminescent ones or light-emitting diodes, when they incorporate photonic crystals or gratings.[25]

Of course these simulations address infinite periodic systems. From the $\Delta\theta \sim 50$ mrad, typical angular width of the lobes on Figs. 6 and 7, it is clear that the emitter size D should verify $D \ll P_{1,2}/\Delta\theta$ to avoid finite size effects and obtain the expected directionality. This means in practice that any size at or above the millimeter range is enough, but that for MEMS oriented applications with, say, $D \sim 100\,\mu$m, finite size effects, e.g., in the form of secondary lobes due to Fourier truncation, should be considered in some detail. Devices with such sizes would correspond to few tens of microwatts in terms of power dissipation by our proposed thermal antennae. Conversely, for macroscopic appliances with power rating in the range 10 mW…100 W, finite size effects are of course irrelevant, only some complexities due to a hierarchy of patterned electrodes needed to spread current at the targeted locations may have to be considered.[25]

IV. THERMAL EMISSION MODULATION

We now investigate the dynamic process of emission of our thermal antenna when an electrode array is voltage-controlled during a given time interval of about 10 μs, which roughly speaking, corresponds, by comparison with the diffusion scale, to 10 times the time needed for heat to be transported over a distance of about 1 μm, the heat capacity and the mass density of VO_2 being $C_{VO_2} = 690\,\mathrm{J\,kg^{-1}\,K^{-1}}$ and $\rho_{VO_2} = 4339\,\mathrm{kg\,m^{-3}}$, respectively.[22] This is typically the deposited layer thickness. Hence, the power dissipated inside

the structure during a half period can be extracted on the back side of the source in a thermalized silicon wafer just underneath the VO_2 layer and at the surface by radiative cooling before a new excitation take places. Hence, after one period all the power dissipated within the structure is extracted from it. By applying a rectangular periodic modulation of the voltage as illustrated in the inset of Fig. 8, the spatio-temporal evolution of temperature field is calculated by solving the heat diffusion equation using a standard finite-element method with an initial temperature $T_0 = 62\,^{\circ}\mathrm{C}$ at any point. In this equation, the thermo-optical coupling results from both the temperature dependence of the surface emissivity of our antenna which controls the cooling of system and from the electrical resistivity (see Fig. 8(d)), which conditions the Joule heating per unit volume.

The thermal emissivity is calculated from the reflection coefficient using the Kirchoff's law. As shown in Fig. 8, the temperature field increases, mostly at the top surface of the source, to generate by phase transition a (non rectangular) grating when the temperature exceeds the critical temperature. By an ad hoc adjustment of the voltage profile applied on the electrodes, we see also that a grating can be periodically inscribed onto the crystalline substrate. Hence, the thermal emission of the source (Fig. 9) changes alternatively

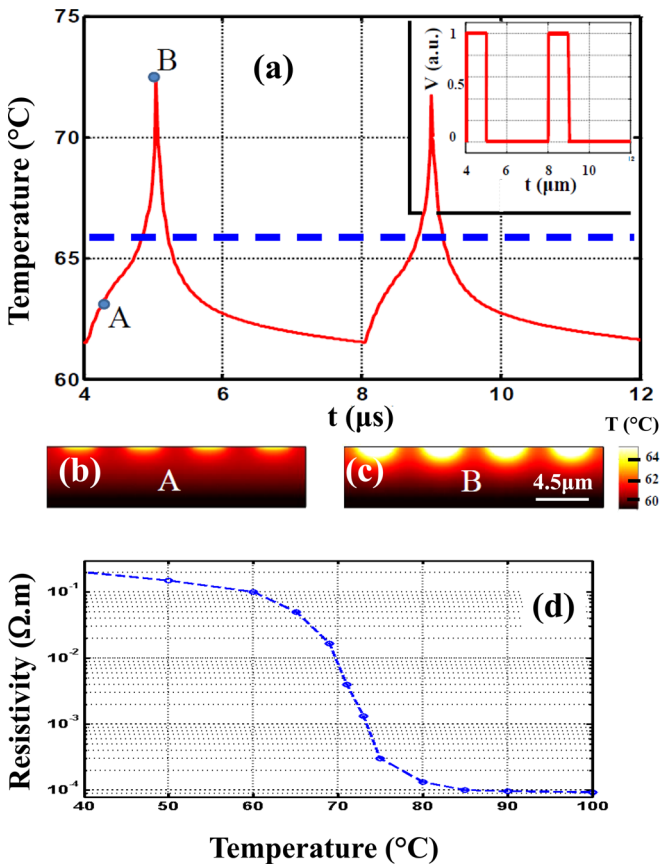

FIG. 8. (a) Time evolution of the maximal temperature in a VO_2 grating with the temporal variation of the voltage applied on each electrode as described in the inset. The horizontal dashed line shows the critical temperature where the transition between the crystalline and the amorphous state takes place. In (b) and (c) are plotted the temperature fields distribution inside the source at two different times. (d) Electrical resistivity of VO_2 used in the model as a function of temperature.[26]

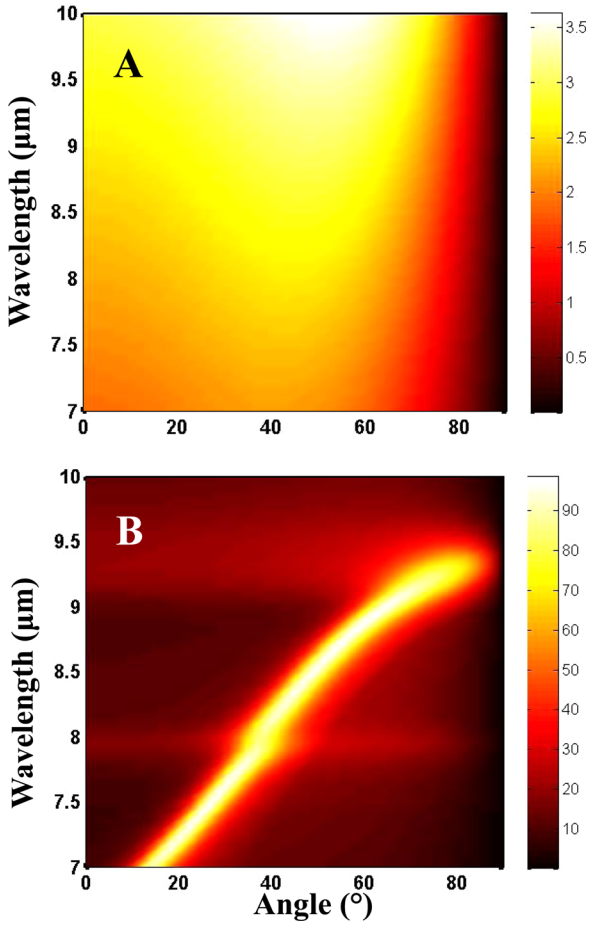

FIG. 9. TM-polarized emissivity (in percent) of the VO_2-source at two different times $t_A = 4.5\ \mu$s and $t_A = 5\ \mu$s as shown in Fig. 8.

between an almost non-emitting behavior and a highly directional and strongly emitting pattern in approximately 0.5 μs. Of course a longer relaxation time (3 μs) is required to cool down the source before applying a new excitation (unlike MEMS, we can cool efficiently by the substrate). Nevertheless, the results plotted in Fig. 9 of emissivity at submicrosecond scale demonstrate unambiguously that our source can operate cyclically at a periodic time of a few microseconds. Moreover, despite the specific shape of the grating unit cell (see Fig. 8(c)), we observe that the emission pattern of the source remains very similar to that of a source having a perfectly rectangular grating as shown in Fig. 6. The differences with the perfect square-pattern lattice for the main Fourier components of the thermally generated grating are thus modest. There is certainly room to optimize the present proposal, especially for targeted applications. But we believe that the proposal as described here is realistic and simple enough to prompt its test and to trigger further progresses.

V. CONCLUSION

In conclusion, we have introduced a switchable thermal antenna based on the phase transition of a polaritonic insulator-metal transition material, namely, the popular vanadium dioxide, a material currently incorporated in many applications such as bolometers and thus well mastered. Our

proposal is very different from any previous one in achieving a quick directional change, thanks to the MIT and voltage-controlled grating. To design switchable antenna that operates at lower or higher temperatures than the critical temperature of VO_2 other carefully chosen MIT materials could of course be used. We have further shown that the thermal emission can be suppressed by the phase transition and that the direction of emission can be tailored by actively changing the geometric features of grating. Applications could cover spectroscopy sources or all kinds of processes with quick surface heating needed.

ACKNOWLEDGMENTS

This work has been partially supported by the Agence Nationale de la Recherche through the Source-TPV Project ANR 2010 BLANC 0928 01.

[1]P. J. Hesketh, J. N. Zemel, and B. Gebhart, Nature **324**, 549–551 (1986).
[2]P. J. Hesketh, J. N. Zemel, and B. Gebhart, Phys. Rev. B **37**, 10803–10813 (1988).
[3]M. Kreiter, J. Oster, R. Sambles, S. Herminghaus, S. Mittler-Neher, and W. Knoll, Opt. Commun. **168**, 117–122 (1999).
[4]J. J. Greffet, R. Carminati, K. Joulain, J. P. Mulet, S. Mainguy, and Y. Chen, Nature **416**, 61 (2002).
[5]O. G. Kollyukh, A. I. Liptuga, V. Morozhenko, and V. I. Pipa, Opt. Commun. **225**, 349 (2003).
[6]P. Ben-Abdallah, J. Opt. Soc. Am. A **21**(7), 1368–1371 (2004).
[7]I. Celanovic, D. Perreault, and J. Kassakian, Phys. Rev. B **72**, 075127 (2005).
[8]B. J. Lee, C. J. Fu, and Z. M. Zhang, Appl. Phys. Lett. **87**, 071904 (2005).
[9]J. Drevillon and P. Ben-Abdallah, J. Appl. Phys. **102**, 114305 (2007).
[10]A. Battula and S. C. Chen, Phys. Rev. B **74**, 245407 (2006).
[11]K. Joulain and A. Loizeau, J. Quant. Spectrosc. Radiat. Transfer **104**(2), 208–216 (2007).
[12]S. Zhang, W. Fan, N. C. Panoiu, K. J. Malloy, R. M. Osgood, and S. R. J. Brueck, Phys. Rev. Lett. **95**, 137404 (2005).
[13]F. M. Wang, H. Liu, T. Li, Z. G. Dong, S. N. Zhu, and X. Zhang, Phys. Rev. E **75**, 016604 (2007).
[14]P. van Zwol, K. Joulain, P. Ben-Abdallah, J. J. Greffet, and J. Chevrier, Phys. Rev. B **83**(20), 201404(R) (2011).
[15]P. van Zwol, K. Joulain, P. Ben-Abdallah, and J. Chevrier, Phys. Rev. B **84**, 161413(R) (2011).
[16]P. Ben-Abdallah and S.-A. Biehs, Appl. Phys. Lett. **103**, 191907 (2013).
[17]P. Ben-Abdallah and S.-A. Biehs, Phys. Rev. Lett. **112**, 044301 (2014).
[18]A. S. Barker, H. W. Verleur, and H. J. Guggenheim, Phys. Rev. Lett. **17**, 1286 (1966).
[19]M. M. Qazilbash, M. Brehm, G. O. Andreev, A. Frenzel, P.-C. Ho, B.-G. Chae, B.-J. Kim, S. J. Yun, H.-T. Kim, A. V. Balatsky, O. G. Shpyrko, M. B. Maple, F. Keilmann, and D. N. Basov, Phys. Rev. B **79**, 075107 (2009).
[20]S.-A. Biehs, P. Ben-Abdallah, F. S. S. Rosa, K. Joulain, and J.-J. Greffet, Opt. Express **19**, A1088–A1103 (2011).
[21]*Handbook of Optical Constants of Solids*, edited by E. Palik (Academic Press, New York, 1998).
[22]J. Chen, X. Liu, X. Yuan, Y. Zhang, Y. Gao, Y. Zhou, R. Liu, L. Chen, and N. Chen, Chin. Sci. Bull. **57**(26), 3393–3396 (2012) and refernces therein.
[23]D.-W. Oh, C. Ko, S. Ramanathan, and D. G. Cahill, Appl. Phys. Lett. **96**, 151906 (2010).
[24]R. Petit, *Electromagnetic Theory of Gratings* (Springer, Berlin, 1980); M. G. Moharam, E. B. Grann, D. A. Pommet, and T. K. Gaylord, J. Opt. Soc. Am. A **12**, 1068–1076 (1995).
[25]A. David, H. Benisty, and C. Weisbuch, Rep. Prog. Phys. **75**, 126501 (2012).
[26]G. Gopalakrishanan, D. Ruzmetov, and S. Ramanathan, J. Mater. Sci. **44**, 5345–5353 (2009).